# Structure of $UC_2$ and $U_2C_3$:XRD, $^{13}C$ NMR and EXAFS study

U. Carvajal Nuñez [a], R. Eloirdi [a,*], D. Prieur [a], L. Martel [a], E. López Honorato [b], I. Farnan [c], T. Vitova [d], J. Somers [a]

[a] European Commission, Joint Research Centre, Institute for Transuranium Elements, P.O. Box 2340, D-76125 Karlsruhe, Germany
[b] Centro de Investigatión y de Estudios Avanzados del IPN (CINVESTAV), Unidad Saltillo, Av. Industria Metalúrgica 1062, Ramos Arizpe, Coahuila 25900, Mexico
[c] University of Cambridge, Cambridge CB2 1TN, UK
[d] Institut für Nukleare Entsorgung (INE), P.O. Box 3640, D- 76021 Karlsruhe, Germany

ARTICLE INFO

*Keywords:*
NMR
EXAFS
XRD
Carbides
Uranium
Nuclear Fuel

ABSTRACT

In this study, uranium dicarbide ($UC_2$) has been prepared by arc melting and heat treated under vacuum to form uranium sequicarbide ($U_2C_3$) in the presence of a second phase $UC_{2-z}$. Both samples, as cast and heat treated, have been characterised by chemical analyses, X ray diffraction (XRD), $^{13}C$ magic angle spin ning nuclear magnetic resonance (MAS NMR) and by extended X ray absorption fine structure (EXAFS). The composition, the purity, the various environments of both U and C atoms as well as the bonds length with the coordination number have been determined. By combining a long range order method (XRD) and short range order spectroscopy techniques (EXAFS and NMR), a unique view on the microstructure of $UC_2$, before and after heat treatment, and of $U_2C_3$ phase has been achieved.

## 1. Introduction

Carbide materials are potential fuels for a number of advanced reactor designs [1] and for propulsion systems [2], as some of their properties are more favourable than oxides based fuels. Indeed, they are known for their high thermal conductivity [3], their higher structural stability and high fusion temperature [4 6]. Given the interest in uranium carbides for nuclear applications, a complete knowledge on the crystallographic properties of these materials is essential. Indeed, the presence of structural defects can affect the fuel properties during irradiation and could lead eventually to a degradation of both reactor safety and fuel performance [7 9]. According to the U C phase diagram [10,11], the main stoichiometries of uranium carbides are uranium monocarbide ($UC_{1\pm x}$ with $x \leqslant 0.05$), uranium sesquicarbide ($U_2C_3$), and uranium dicarbide ($UC_2$). In our previous study [12] on $UC_{1\pm x}$, we investi gated its structure with XRD, NMR and EXAFS techniques. It was possible to probe order disorder transition affected by the carbon content and the heat treatment. In this paper we extend this study to $UC_2$ and $U_2C_3$, the two other phases of the U C system. Based on literature and the phase diagram, $UC_2$ phase exists in two different structures, a tetragonal form with a $CaC_2$ structure type (I4/mmm, space group (SG) n°139) [13,14] at lower temperature denoted α UC2 and a cubic form with a NaCl structure type (Fm 3m, SG n°225) at higher temperatures, denoted the β UC2. $UC_2$, when synthesised, is always sub stoichiometric with a com position domain ranging from $UC_{1.75}$ to $UC_{1.95}$ [3]. The lattice parameter increases with the carbon content and with heat treat ment [15]. The $U_2C_3$ phase has the body centred cubic $Pu_2C_3$ type structure (I 43d, SG n°220) [13,14] and cannot be obtained directly by arc melting [3]. Many controversies have been reported in the literature on the synthesis of $U_2C_3$ [16] and its magnetic properties [17]. Now it is well known that $U_2C_3$ can be generated from a start ing material $UC_x$ ($x$ = 1.5 2) by grinding, pressing, and heating un der high vacuum. Obtaining $U_2C_3$ as a single phase is difficult most likely due to the slow kinetics of the reaction. According to the starting composition, two mechanisms of reaction can take place to synthesize it, the synthetic and the decomposition reaction [18] described in Eqs. (1) and (2) respectively:

$$UC_2 + UC \rightarrow U_2C_3 \quad (1)$$

$$2UC_2 \rightarrow U_2C_3 + C \quad (2)$$

The decomposition reaction is slower than the synthetic reaction [19] and requires high vacuum to induce the departure of oxygen which in fact stabilises $UC_2$ [20]. Nickel and Saeger [19] argued that pure $UC_2$ sample does not lead directly to sesqui carbide (Eq. (2)) but it decomposes first following the reaction: $UC_2 \rightarrow UC + C$. If this is correct, then the intermediate UC should appear and should be detected by XRD and/or NMR, provided it is not consumed quickly. Thus, in this study we investigate the

* Corresponding author. Tel.: +49 7247951 803; fax: +49 7247951 599.
*E-mail address:* rachel.eloirdi@ec.europa.eu (R. Eloirdi).

decomposition reaction starting with a C/U composition close to the $UC_2$ compound. While static $^{13}C$ NMR studies have been reported on $UC_2$ and $U_2C_3$ in the past [21,22], so far no MAS NMR and no EXAFS studies have been performed on any of these phases. Chemical analyses inform us about the carbon content, XRD about the nature of the present phases, EXAFS will inform us about the bond distances in $U_2C_3$, in $UC_2$ as cast and heat treated, whereas NMR provides information on the different C environments. In the present work, we will first focus on the local structure of $UC_2$ as cast and then on $UC_2$ pressed and heat treated under high vacuum inducing the formation of $U_2C_3$ through an investigation coupling XRD, EXAFS and $^{13}C$ MAS NMR.

## 2. Experimental

### 2.1. Synthesis

The sample of uranium dicarbide $UC_2$ was prepared by arc melting of uranium metal and graphite under a high purity argon atmosphere (6 N) on a water-cooled copper hearth. Zirconium was placed in the preparation chamber and served as a getter for oxygen and nitrogen. The uranium dicarbide ingot was melted and turned around several times to achieve a homogenous sample. Synthesis of uranium sesquicarbide $U_2C_3$ is achieved by the heat treatment of the $UC_2$ sample. The latter was ball milled, pelletized and heat treated at 1450 °C for 48 h under high vacuum ($10^{-5}$ mbar) followed by a slow cooling at 20 °C $h^{-1}$. In this article, the term "$U_2C_3$" is used to describe the sample obtained after heat treatment of $UC_2$ pellet and corresponds to a mixture of $U_2C_3$ and $UC_{2-z}$ phases. As carbides are easily oxidised in presence of humidity [23,24], the as-synthesized samples were stored under helium (6 N) to minimise oxygen contamination before performing the measurements.

### 2.2. Sample characterization methods

#### 2.2.1. Chemical analysis

Chemical analyses of carbon contents have been performed on powdered samples by direct combustion using the infrared absorption detection technique with an ELTRA CS-800 instrument.

#### 2.2.2. X-ray diffraction

X-ray diffraction analysis was performed on a Bruker D8 Bragg–Brentano advanced diffractometer (Cu $K\alpha_1$ radiation) equipped with a Lynxeye linear position sensitive detector and installed inside a glove box under inert atmosphere. The powder diffraction patterns were recorded at room temperature using a step size of 0.01973° with an exposure of 4 s across the angular range $20° \leqslant 2\theta \leqslant 120°$. The operating conditions were 40 kV and 40 mA. Lattice parameters and quantification of the "$U_2C_3$" sample was performed by Rietveld refinement using Topas 4.1. software [25].

#### 2.2.3. Nuclear magnetic resonance (NMR)

Uranium carbide ingots were crushed to a fine powder and loaded into 1.3 mm zirconia rotors under helium (6 N) in a glove box. The particle size was sufficiently small not to affect the radiofrequency response of the sample due to skin-depth effects. The $^{13}C$ NMR spectra, with $^{13}C$ in natural abundance (1.1%), were recorded on a Bruker Advance 400 spectrometer operating at 9.4 T (Larmor frequency of $^{13}C$ 100 MHz). This apparatus has been adapted for the study of highly radioactive material using commercial NMR probes and rotors [26]. Despite the potential for eddy current effects during spinning of the semi-metallic uranium carbides, most of the $^{13}C$ MAS-NMR spectra were acquired at spinning rates of 55 kHz. A rotor-synchronised Hahn echo was used to acquire the spectra. In order to minimise baseline distortions the pulse durations were 2.5 μs ($\pi/2$) and 5 μs ($\pi$), respectively, with an echo delay of 18.2 μs (1 rotor period). Fully relaxed spectra could be acquired with a recycle delay of 150 ms due to the efficient paramagnetic relaxation mechanism provided by the conduction electrons [27]. $^{13}C$ chemical shifts were calibrated relative to tetramethylsylane (0 ppm) by using adamantane as a secondary reference, with $^{13}CH$ and $^{13}CH_2$ peaks at 29.45 ppm and 38.48 ppm [28], respectively. Due to safety restrictions on running the MAS-NMR system unattended overnight, the number of transients was limited to 51,200 for each spectrum. All the spectra were fitted using the DMFIT software [29].

#### 2.2.4. Extended X-ray absorption fine structure

EXAFS measurements were performed on the uranium carbides powder co-milled with BN at the INE-Beamline at the Angströmquelle Karlsruhe (ANKA) [30]. A Ge(422) double crystal monochromator coupled with a collimating and focusing Rh-coated mirrors was used. X-ray absorption fine structure (XAFS) spectra were collected in transmission geometry at the U $L_{III}$ (17,166 eV) edge. Energy calibration was provided by an yttrium (17,038 eV) foil located between the second and the third ionization chamber. Each spectrum was aligned using the U reference foil XANES spectra before averaging scans. The ATHENA software [31] was used for data reduction, normalisation and extraction of EXAFS oscillations. Experimental EXAFS spectra were Fourier-transformed using a Hanning window within 2.5–8.8 $Å^{-1}$ $k$-range. The ARTEMIS software [31] was used to perform the fits. Both scattering phases and amplitudes were calculated using the *ab initio* code FEFF8.20 [32]. Data fitting was performed in $R$ space for $R$ values ranging from 1.4 to 5.1 Å. The $S_0^2$ value was set at 0.9 and the shift in threshold energy was varied as a global parameter.

## 3. Results and discussion

### 3.1. Chemical and X ray diffraction analyses of $UC_2$ as cast and "$U_2C_3$" samples

The chemical analysis results, summarized in Table 1, indicate that the as cast $UC_2$ sample has a carbon content of 8.70 ± 0.26 wt% corresponding to a stoichiometry of $UC_{1.89\pm0.06}$. Within uncertainty of the measurement this stoichiometry lies within the theoretical value derived from the starting material, i.e. $UC_{1.94}$. This slight hypostoichiometry was expected however, as the composition domain of $UC_2$ ranges from $UC_{1.75}$ to $UC_{1.95}$ [3]. In the present manuscript, the nomenclature of the hypostoichiometric and as cast sample $UC_{1.94}$ will be simply $UC_2$. Also the analyses show that after heat treatment of pressed $UC_2$, the carbon content in "$U_2C_3$" sample decreased. This carbon can leave the matrix as CO through the application of the temperature and the high vacuum [33,34].

All peaks in the XRD pattern of the $UC_2$ sample, presented in Fig. 1 (insert), could be assigned to a tetragonal structure and a space group of I4/mmm. It shows that uranium dicarbide can be obtained directly as a single phase in this composition domain by arc melting. The broadening of the peaks, related to the crystallite size and the strain [35] present in the material, is linked out to the preparation using ball milling [36]. The high purity of the sample is also supported by the low oxygen content (<200 ppm). The associated lattice parameters were $a = 3.5225\ (1)$ Å and $c = 5.994\ (1)$ Å, which are in good agreement with literature data [37,38].

**Table 1**
Chemical analyses of $UC_2$ as cast and "$U_2C_3$" samples.

| | $UC_2$ | "$U_2C_3$" |
|---|---|---|
| Theoretical C content (wt%) | 8.91 | – |
| C/U ratio | 1.94 | – |
| Measured C content (wt%) | 8.70 (0.26) | 8.20 (0.16) |
| C/U ratio | 1.89 (0.06) | 1.77 (0.04) |

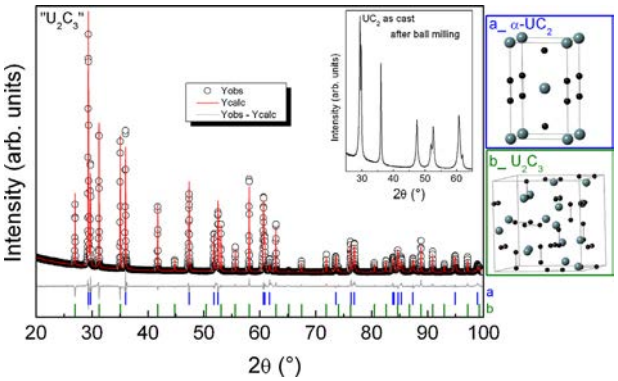


**Fig. 1.** Rietveld refinement of "$U_2C_3$" X-ray diffraction pattern (blue stick corresponding to $UC_2$ phase and green stick corresponding to $U_2C_3$ phase with their corresponding crystalline structure)_insert: XRD pattern of $UC_2$ as cast. (For interpretation of the references to colour in this figure legend, the reader is referred to the web version of this article.)

After ball milling and pressing of the as cast $UC_2$ sample, the heat treatment at 1450 °C 48 h under high vacuum lead to the formation of a mixed phase sample, whose X ray diffraction pattern is presented in Fig. 1. All the peaks have been assigned to two phases, $U_2C_3$ with body centred cubic $Pu_2C_3$ type (I 43d) and $UC_{2-z}$ with tetragonal structure, with an approximate composition of about 30 and 70 wt% respectively, as determined by Rietveld refinement. This composition is also supported by the phase rule, considering the phase diagram [11] and the C/U ratio of the sample ($UC_{1.77\pm0.04}$) determined by chemical analyses. The lattice parameter of $U_2C_3$, $a$ = 8.0889 (3) Å, is in good agreement with literature data [30]. The lattice parameters of $UC_{2-z}$ after annealing increase to $a$ = 3.5252(3) Å and $c$ = 6.000 (2) Å.

### 3.2. Local structure

#### 3.2.1. Study of $UC_2$ as cast sample

The fitted U $L_{III}$ edge EXAFS spectra in $k$ and $R$ space are presented in Fig. 2. The calculated $UC_2$ crystallographic parameters are given in Table 2. Taking into account the results of the XRD analysis, the EXAFS experimental data were fitted using a model consisting of spherical cluster of atoms with 7.5 Å size and $CaC_2$ type structure (I4/mmm). The following single scattering paths were taken into account: 2 U C, 1 U U and 1 U C, 1 U U corresponding to the first and second U coordination spheres, respectively. Both triangular and quadruple multiple scattering paths were included in the fit. The EXAFS analyses indicate that U is surrounded by C atoms at 2.30 (1), 2.58 (1) and 3.71 (3) Å and by U atoms at 3.53 (1) and 3.87 (1) Å. The U $U_1$ distance, corresponding to the lattice parameter a, is in good agreement with the value derived from XRD. From these derived interatomic distances, one can calculate that the C C distance of the $C_2$ dumbbells is equal to 1.39 (1) Å, which is slightly higher than the previous reported value of 1.37 (1) Å [39].

In Fig. 3, the $^{13}C$ Hahn echo MAS NMR spectrum of $UC_2$ acquired at a spinning frequency of 55 kHz is presented. As the uranium carbides are semi metals, large NMR shifts (Knight shifts) are expected due to the collective hyperfine shifts of unpaired electrons near the Fermi surface [40]. The spectrum has been fitted with two Gaussians at 1522 (70) ppm ($C_\beta$) and 1362 (10) ppm ($C_\alpha$) with full width at half maxima (FWHM) of 215 (4) and 142 (1) ppm, respectively (see Table 3. Additional spinning sidebands have been identified and are indicated by stars. The second carbon environment, $C_\beta$, was detected with an intensity corresponding to 30% of the total spectrum area. $C_\alpha$ could be attributed to carbons localized on the octahedral sites of the $CaC_2$ structure while $C_\beta$ to carbons in a more disordered environment (i.e. due to the presence of more vacancies or interstitials due to the rapid cooling). The value of the $^{13}C$ shifts found here are relatively similar to that found by Lewis et al. [22] (Fig. 3B), who, only identified one peak, probably due to the low signal to noise ratio.

To induce improved local ordering of the carbons as previously seen for $UC_{0.96}$ [12], an annealing of an ingot piece of $UC_2$ was made for 10 h at 1450 °C. The ordering of the structure in $UC_2$ (release of strain, vacancies ordering) should have led to a decrease of the $C_\beta$ peak intensity and width. Unfortunately, however, the annealed sample would not spin for further MAS NMR analysis. This could have been due to an increased metallic property inducing a higher Eddy current and preventing the rotation of the sample in high field, as one might expect, as it has been shown that the resistivity of $UC_2$ decreases after annealing [41]. A static experiment (Fig. 4) performed on the same sample shows a narrowing and a better resolution of the peaks $C_\alpha$ and $C_\beta$ in the annealed sample in agreement with an ordering of the structure. Also the heat treatment

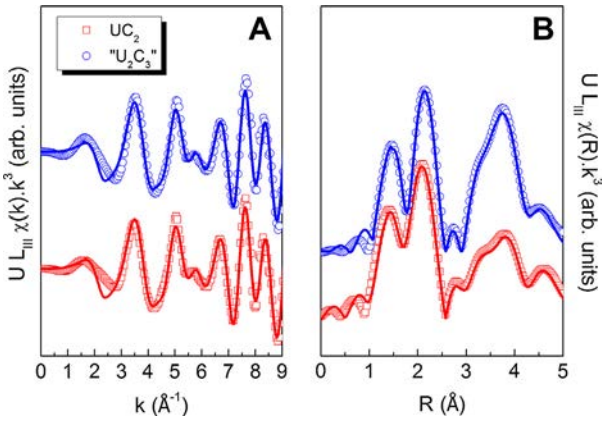


**Fig. 2.** Experimental U–$L_{III}$ EXAFS spectra and their corresponding Fourier transforms of $UC_2$ as cast and "$U_2C_3$" samples.

**Table 2**
Crystallographic parameters derived from EXAFS analyses of $UC_2$ as cast sample($R$: interatomic distance; $N$: number of neighbours; $\sigma$: Debye–Waller factor, (a) this work, (b) calculated data [39]).

| Shell | $R$ (Å) | | $N$ | $\sigma$ (Å$^2$) | $R$ factor (%) |
|---|---|---|---|---|---|
| | (a) | (b) | (a) | (a) | |
| U–$C_{1a}$ | 2.30 (1) | 2.32 | 2 | 0.0073 (3) | 2.1 |
| U–$C_{1b}$ | 2.58 (1) | 2.59 | 8 | 0.0071 (6) | |
| U–$U_1$ | 3.53 (1) | 3.54 | 4 | 0.0040 (4) | |
| U–$C_2$ | 3.71 (3) | 3.88 | 2 | 0.008 (1) | |
| U–$U_2$ | 3.87 (3) | 3.90 | 8 | 0.006 (2) | |

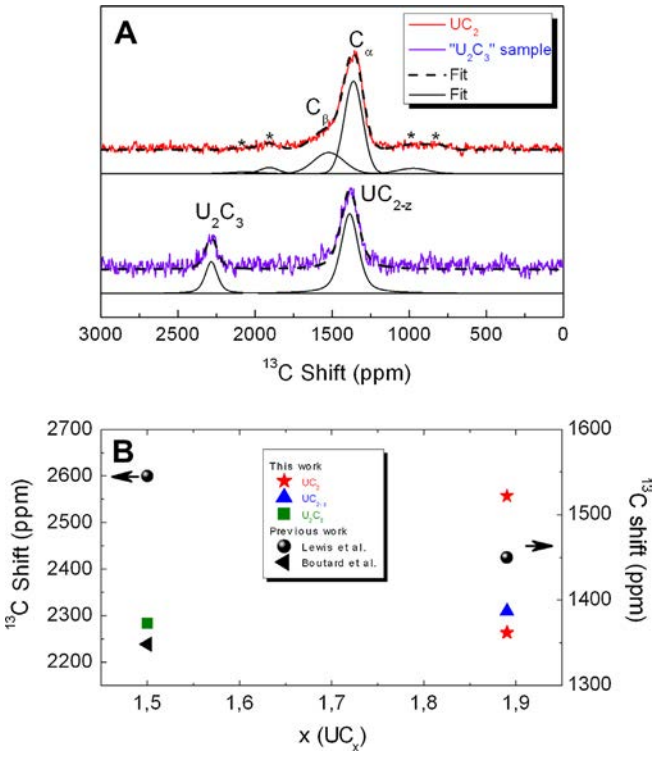


**Fig. 3.** A. $^{13}C$ Hahn-echo MAS-NMR spectra of $UC_2$ and "$U_2C_3$" samples obtained at a spinning frequency of 55 kHz ($B_0$ = 9.4T). The "$U_2C_3$" sample contains $U_2C_3$ and $UC_{2-z}$ phases. The stars correspond to the spinning sidebands. B. Comparison with literature of $^{13}C$ shifts in $UC_2$ and $U_2C_3$.

**Table 3**
$^{13}C$ isotropic chemical shift ($\delta_{iso}$), content of each $^{13}C$ species and Full Width at Half Maximum (FWHM) for the as cast $UC_2$ and "$U_2C_3$" samples acquired at a spinning frequency of 55 kHz. (For $UC_2$:$C_\alpha$:$\delta_{iso}$ of the main peak and $C_\beta$:$\delta_{iso}$ of the second peak).

| Sample | $\delta_{iso}$ (ppm) | | Content (mol%) | | FWHM (ppm) | |
|---|---|---|---|---|---|---|
| | $^{13}C_\beta$ | $^{13}C_\alpha$ | $^{13}C_\beta$ | $^{13}C_\alpha$ | $^{13}C_\beta$ | $^{13}C_\alpha$ |
| $UC_2$ | 1522 (70) | 1362 (10) | 30 | 70 | 215 (4) | 142 (1) |
| "$U_2C_3$" | $^{13}C_{U2C3}$ 2283 (50) | $^{13}C_{UC2\ z}$ 1387 (10) | $^{13}C_{U2C3}$ 25 | $^{13}C_{UC2\ z}$ 75 | $^{13}C_{U2C3}$ 106 (2) | $^{13}C_{UC2\ z}$ 148 (1) |

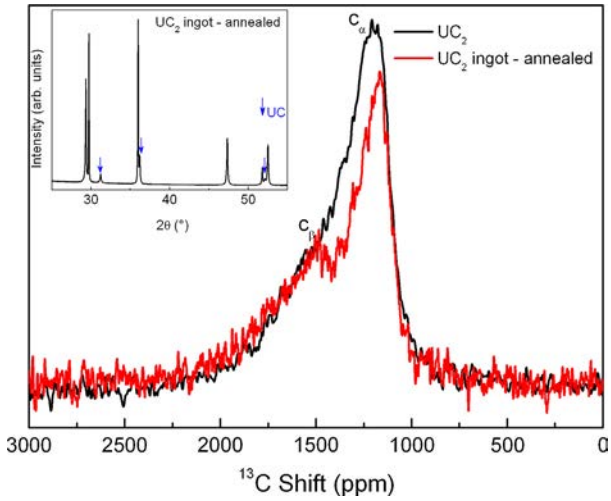


**Fig. 4.** $^{13}C$ Hahn-echo static spectra of $UC_2$ as cast and of an ingot piece of $UC_2$ annealed at 1450 °C for 10 h at 10 $^{5}$ mbar ($B_0$ = 9.1T).

**Table 4**
Crystallographic parameters derived from EXAFS analyses of $U_2C_3$ phase present in the "$U_2C_3$" sample ($R$: interatomic distance; $N$: number of neighbours; $\sigma$: Debye–Waller factor, (a) this work, (b) calculated data [39]).

| Shell | $R$ (Å) | | $N$ | $\sigma$ (Å$^2$) | $R$ factor (%) |
|---|---|---|---|---|---|
| | (a) | (b) | (a) | (a) | |
| U–$C_{1a}$ | 2.45 (2) | 2.50 | 3 | 0.0075 (4) | 2.5 |
| U–$C_{1b}$ | 2.57 (2) | 2.56 | 3 | 0.0078 (5) | |
| U–$C_{1c}$ | 2.77 (2) | 2.82 | 3 | 0.0076 (3) | |
| U–$U_{1a}$ | 3.35 (3) | 3.34 | 3 | 0.005 (1) | |
| U–$U_{1b}$ | 3.53 (3) | 3.48 | 2 | 0.004 (2) | |
| U–$U_{1c}$ | 3.70 (5) | 3.68 | 6 | 0.005 (2) | |

made on ingot of $UC_2$ lead to lattice parameters of $a$ = 3.5280(1) Å, $c$ = 6.008 (6) Å and to the precipitation of UC (as shown in the XRD data in the insert in Fig. 4), showing that the process of grinding and pressing is indeed necessary to form $U_2C_3$ [42]. In our previous study [12], static spectrum of UC displayed a $^{13}C$ shift of 1464 ppm. It overlaps with the $C_\beta$ peak of $UC_2$, and thus we cannot distinguish the two phases (UC and $C_\beta$ of $UC_2$) by this technique. The precipitation of UC in annealed ingot of $UC_2$ sample has been reported in literature [19,43] and no explanation concerning the absence of $U_2C_3$ formation through synthetic reaction was provided so far.

### 3.2.2. Study of "$U_2C_3$" sample

The U $L_{III}$ edge spectra of the "$U_2C_3$" sample in $k$ and $R$ space are plotted in Fig. 2. The FT spectra of "$U_2C_3$" and $UC_2$ (Fig. 2B) differ in the 3 5 Å $R$ range due to variations of the number of U atoms in the second shell. The crystallographic parameters of $U_2C_3$ and $UC_{2\ z}$ are summarized in Table 4 and Table 5, respectively. Both $U_2C_3$ and $UC_{2\ z}$ crystal phases were taken into account in the structural

**Table 5**
Crystallographic parameters derived from EXAFS analyses of $UC_{2\ z}$ phase present in the "$U_2C_3$" sample ($R$: interatomic distance; $N$: number of neighbours; $\sigma$: Debye–Waller factor, (a) this work, (b) calculated data [39]).

| Shell | $R$ (Å) | | $N$ | $\sigma$ (Å$^2$) | $R$ factor (%) |
|---|---|---|---|---|---|
| | (a) | (b) | (a) | (a) | 2.3 |
| U–$C_{1a}$ | 2.31 (2) | 2.32 | 2 | 0.008 (1) | |
| U–$C_{1b}$ | 2.58 (2) | 2.59 | 8 | 0.008 (1) | |
| U–$U_1$ | 3.54 (2) | 3.54 | 4 | 0.005 (1) | |
| U–$C_2$ | 3.72 (3) | 3.88 | 2 | 0.009 (1) | |
| U–$U_2$ | 3.89 (3) | 3.90 | 8 | 0.007 (2) | |

model used in the EXAFS analyses. Spherical clusters of 7.5 Å in size with a $Pu_2C_3$ type structure (I 43d, $U_2C_3$) and $CaC_2$ type structure (I4/mmm, $UC_2$) were employed in the FEFF calculations.

The experimental data and fit agree within 2.5%, which confirms the validity of the used models. The interatomic distances derived from EXAFS are well in accordance with first principle calculation made by Shi et al. [39] on $U_2C_3$. Indeed, the first U C interatomic distances are equal to 2.45 (2), 2.57 (2) and 2.77 (2) Å. The U U interatomic distances are equal to 3.35 (3), 3.53 (3) and 3.70 (5) Å respectively (see Tables 4 and 5). Regarding the $UC_{2\ z}$ phase, the interatomic distances seem slightly larger than those observed in the as cast $UC_2$ sample. Although the experimental error is significant, these EXAFS results are consistent with the increase of the lattice parameters observed by XRD.

Fig. 3A (bottom) presents the $^{13}C$ Hahn echo MAS NMR spectrum of "$U_2C_3$" acquired at spinning frequency of 55 kHz. Two peaks are identified, one at 1387 (10) ppm and another at 2283 (50) ppm. The first peak is attributed to $UC_{2\ z}$ based on the previous NMR spectrum (Fig. 3A (top)) and on XRD data. It should be noticed that the peak is slightly shifted (~30 ppm) compared to that of the as cast $UC_2$ sample. This difference should be due to a different carbon environment characterised by a different lattice parameters. The second peak can be attributed to $U_2C_3$ phase. Its shift is lower than that obtained in the static experiment by Lewis et al. [22], but very close to that obtained by Boutard and De Novion [21] (Fig. 3B). The quantification of the two phases as obtained by NMR ($UC_{2\ z}$/$U_2C_3$: 75 mol%/25 mol%) confirms that derived from XRD analysis ($UC_{2\ z}$/$U_2C_3$: 70 wt%/30 wt%). If free carbon is present in the sample, it is below the detection limits of both NMR and XRD. The "$U_2C_3$" sample has a carbon content of 8.20 ± 16 wt%, and it has been reported [18] that free carbon appears in samples containing more than 8.6 wt% of C.

### 3.2.3. Synthesis mechanism of $U_2C_3$ from $UC_2$

Taking into account the quantification of the two phases obtained by XRD ($UC_{2\ z}$/$U_2C_3$: 70 wt%/30 wt%), the carbon content in "$U_2C_3$" sample determined by chemical analyses (Table 1) and considering the atomic mass of carbon is negligible relative to uranium so that in terms of molar mass $M_{UC2\ z} \sim ½\ M_{U2C3} \sim M_{UC1.77}$, then one finds that the C/U ratio of $UC_{2\ z}$ is about 1.89. This value is, within the experimental error of the chemical analysis, identical

to the starting $UC_2$ as cast sample. Thus under our experimental conditions, we can represent the reaction of the crushed and pel letized sample under heat treatment ($\Delta$) at 1450 °C, during 48 h and $10^{-5}$ mbar nominally as,

$$UC_2(UC_{1.89}) \xrightarrow{\Delta} 0.12\ \overset{\nearrow}{C} + \text{“}U_2C_3\text{”}(UC_{1.77}) \quad UC_{2-z}(UC_{1.89}) + U_2C_3$$

We can also exclude that the ratio C/U in $UC_{2-z}$ is superior to the ratio present in the starting material $UC_2$. Indeed, as argued Imoto et al. [18], this should only take place when UC precipitates after heat treatment of $UC_2$, just as we observed when heating an ingot of $UC_2$ (Fig. 4).

The carbon content decrease is related to the decarburisation of $UC_2$ which can take place along reactions (3) and (4), having the change in Gibbs free energy as reported in reference [44]:

$\Delta G_f^{deg}$ (1300 K) [44]

$$2UC_2 \rightarrow U_2C_3 + C \qquad 7.9\ \text{kJ/mole} \tag{3}$$

$$UC_2 \rightarrow UC + C \qquad 3.8\ \text{kJ/mole} \tag{4}$$

when reaction (4) occurs, UC could react along two reaction paths, (5) and (6), to form $U_2C_3$:

$$UC + UC_2 \rightarrow U_2C_3 \qquad 2.9\ \text{kJ/mole} \tag{5}$$

$$2UC + C \rightarrow U_2C_3 \quad + 2.1\ \text{kJ/mole} \tag{6}$$

Reaction (6) is from a thermodynamic perspective not favour able and thus if UC is present then it contributes only to the forma tion of $U_2C_3$ via the synthetic reaction (5). Within the detection limit of XRD, we did not observe a UC phase as an intermediate on heating a pellet formed from a crushed sample and this may ex clude the process of synthetic reaction as a requirement for the decomposition reaction, as has been proposed by Nickel and Saeger [19]. The detection limit of XRD and NMR, however, does not exclude the later assumption completely. Nevertheless, the precip itation of UC in a matrix of $UC_2$, when heating an as cast ingot di rectly, does not lead to the formation of $U_2C_3$ (Fig. 4). The grinding and the pressing of $UC_2$ before heat treatment are essential to syn thesize $U_2C_3$.

Apart from the slow rate of the decomposition reaction, the $U_2C_3$ yield may be limited due to either insufficient oxygen in the sample to remove C as CO and possibly drive the reaction. It could also be speculated that the absence of excess carbon in the starting material to precipitate the C in the sample could hinder the reaction. Monitoring the reaction as a function of time would be necessary, together with an analysis of the gas formed during the reaction, to elucidate this matter.

It is interesting to note, however, that the heat treatment on the $UC_2$ pellet (Fig. 1), leads to a highly crystallised “$U_2C_3$” sample as displayed by very narrow diffraction peaks. The thermal energy obviously permits C diffusion and the growth of $U_2C_3$ crystallites during the process [42,45,46].

## 4. Conclusion

A structural investigation of $UC_2$ (=$UC_{1.89\pm0.05}$) and $U_2C_3$ phases has been performed using a unique combination of different tech niques (XRD, NMR and EXAFS). $UC_2$ can be obtained directly by arc melting. EXAFS determination of the first U–C and U–U bond dis tances is in agreement with the tetragonal $CaC_2$ structure. $^{13}C$ MAS NMR of the $UC_2$ sample identified a major carbon contribution at 1362 ppm, and a small contribution to the signal at 1522 ppm, which we attribute to a well ordered and less ordered phases, respectively. Heat treatment of such as cast ingots results in its partial decomposition to UC. In contrast heat treatment of a pulverised ingot, repressed into a pellet yields a $U_2C_3$ phase coex isting with a second phase of $UC_{2-z}$, with the latter having a slightly different lattice parameter than the as cast sample. EXAFS studies could distinguish between the $CaC_2$ and $Pu_2C_3$ type phase's present, while $^{13}C$ NMR identified the shift of the $U_2C_3$ at 2283 ppm. The mechanisms of the reaction leading to $U_2C_3$ are not clear, but the results of this study suggest that a simple decom position mechanism is most likely.

## Acknowledgments

The authors thank T. Charpentier for fruitful discussion, Chris Selfslag, D. Boüxière, C. Boshoven and S. Morel for their technical help at the Institute for Transuranium Elements (ITU). The authors are also grateful to ANKA for providing beamtime and, especially, thank K. Dardenne and J. Rothe for their support during XAS experiments.

## References

[1] M.K. Meyer, R. Fielding, J. Gan, J. Nucl. Mater. 371 (2007) 281–287.
[2] D.R. Koenig, LANL LA-10062-H, 1986.
[3] B.R.T. Frost, J. Nucl. Mater. 10 (1963) 265–300.
[4] H. Matsui, J. Nucl. Sci. Technol. 9 (1972) 185–186.
[5] A.S. Kolokol, A.L. Shimkevich, Int. Conf. Nucl. Eng., Proceedings, ICONE 1 (2008) 759–763.
[6] P. Rodriguez, Bull. Mater. Sci. 22 (1999) 215–220.
[7] F.J. Homan, T.B. Lindemer, E.L. Long, T.N. Tiegs, R.L. Beatty, Nucl. Technol. 35 (1977) 428–441.
[8] K. Minato, T. Ogawa, K. Sawa, A. Ishikawa, T. Tomita, S. Iida, H. Sekino, Nucl. Technol. 130 (2000) 272–281.
[9] E.K. Storms Jr., E.J. Huber, J. Nucl. Mater. 23 (1967) 19–24.
[10] P.-Y. Chevalier, E. Fischer, J. Nucl. Mater. 288 (2001) 100–129.
[11] D. Manara, F. De Bruycker, A.K Sengupta, R. Agarwal, H.S Kamath, in: R. Konings (Ed.), Comprehensive Nuclear Materials, Elsevier, Amsterdam, Holland, 2012, pp. 87–137.
[12] U. Carvajal-Nunez, L. Martel, D. Prieur, E. Lopez Honorato, R. Eloirdi, I. Farnan, T. Vitova, J. Somers, Inorg. Chem. 52 (2013) 11669–11676.
[13] C. De Novion, J.-P. Krebs, P. Meriel, C.R. Acad. Sci. Paris, Ser. B 263 (1966) 457–459.
[14] A.E. Austin, Acta Crystallogr. 12 (1959) 159–161.
[15] H. Tagawa, K. Fujii, Y. Sasaki, J. Nucl. Sci. Technol. 8 (1971) 244–249.
[16] A. Buschinelli, A. Naoumidis, H. Nickel, J. Nucl. Mater. 58 (1975) 67–77.
[17] R. Eloirdi, A.J. Fuchs, J.-C. Griveau, E. Colineau, A.B. Shick, D. Manara, R. Caciuffo, Phys. Rev. B 87 (2013) 214414-1–214414-9.
[18] S. Imoto, T. Sano, Y. Takada, K. Yamamoto, K. Watanabe, T. Isoda, H. Uchikoshi, in: L.E. Russell et al. (Eds.), Carbides in Nuclear Energy, vol. 1, Maunillan, London, 1964, pp. 7–21.
[19] H. Nickel, H. Saeger, J. Nucl. Mater. 28 (1968) 93–104.
[20] J. Henney, D.T. Livey, N.A. Hill, Trans. Brit. Ceram. Soc. 62 (1963) 955.
[21] J.-L. Boutard, C.-H. De Novion, Solid State Commun. 14 (1974) 181–185.
[22] W.B. Lewis, S.W. Rabideau, N.H. Krikorian, W.G. Witteman, Phys. Rev. 170 (1968) 455–462.
[23] L.J. Colby Jr., J. Less Common Metals 10 (1966) 425–431.
[24] A. Schürenkämper, J. Inorg. Nucl. Chem. 32 (1970) 417–429.
[25] A. Coelho, TOPAS-Academic, V. 4.1, Coelho Software, Brisbane, 2007.
[26] L. Martel, J. Somers, C. Berkmann, F. Koepp, A. Rothermel, O. Pauvert, C. Selfslag, I. Farnan, Rev. Sci. Instrum. 84 (2013) 55112–55112-5.
[27] C.P. Slichter, Principles of Magnetic Resonnance; 1980th ed.; Springer-Verlag, New York.
[28] C.R. Morcombe, K.W. Zilm, J. Magn. Reson. 162 (2003) 479–486.
[29] D. Massiot, F. Fayon, M. Capron, I. King, S. Le Calvé, B. Alonso, J.-O. Durand, B. Bujoli, Z. Gan, G. Hoatson, Magn. Reson. Chem. 40 (2002) 70–76.
[30] J. Rothe, S. Butorin, K. Dardenne, M.A. Denecke, B. Kienzler, M. Löble, V. Metz, A. Seibert, M. Steppert, T. Vitova, C. Walther, H. Geckeis, Rev. Sci. Instrum. 83 (2012) 43105–43117.
[31] B. Ravel, M. Newville, J. Synchrotron Radiat. 12 (2005) 537–541.
[32] J.J. Rehr, A. Ankudinov, S.I. Zabinsky, Catal. Today 39 (1998) 263–269.
[33] K. Maruya, S. Takahashi, J. Nucl. Sci. Technol. 5 (1968) 605–609.
[34] V.K. Orlov, V.S. Sergeev, M.A. Fomishkin, A.A. Rostovtsev, A.K. Kruglov, Atomic Energy 95 (2003) 536–539.
[35] M.A. Meyers, A. Mishra, D.J. Benson, Prog. Mater. Sci. 51 (2006) 427.
[36] J.S. Benjamin, T.E. Volin, Metall. Trans. 5 (1974) 1929–1931.
[37] V.V. Akhachinskii, S.N. Bashlykov, Atomic Energy 27 (1969) 524–532.
[38] J. Henney, D.T. Livey, N.A. Hill, Trans. Brit. Ceram. Soc. 62 (1963) 955–973.
[39] H. Shi, P. Zhang, S.-S. Li, B. Wang, B. Sun, J. Nucl. Mater. 396 (2010) 218–222.
[40] S.G. Levine, J. Chem. Educ. 78 (2001) 133.

[41] M. Horiki, S. Miyama, H. Matsui, T. Kirihara, J. Nucl. Sci. Technol. 19 (1982) 83–86.
[42] J. Laugier, P.L. Blum, J. Nucl. Mater. 39 (1971) 245–252.
[43] T. Kurasawa, H. Watanabe, T. Kikuchi, J. Nucl. Mater. 43 (1972) 192–204.
[44] M.C. Krupka, Ceram. Bull. 48 (1969) 1133–1136.
[45] L.M. Litz, A.B. Garrett, F.C. Croxton, J. Am. Chem. Soc. 70 (1948) 1718–1722.
[46] A.E. Austin, A.F. Gerds, The Uranium–Nitrogen–Carbon System, Battelle Memorial Institute, 1958.

Karlsruher Institut für Technologie

OPEN ACCESS

# Repository KITopen

Dies ist ein Postprint/begutachtetes Manuskript.

Empfohlene Zitierung:

Carvajal Nunez, U.; Eloirdi, R.; Prieur, D.; Martel, L.; Lopez Honorato, E.; Farnan, I.; Vitova, T.; Somers, J.
Structure of $UC_2$ and $U_2C_3$:XRD, $^{13}C$ NMR and EXAFS study
2014. Journal of alloys and compounds, 589, 234–239.
doi:10.5445/IR/110098704

Zitierung der Originalveröffentlichung:

Carvajal Nunez, U.; Eloirdi, R.; Prieur, D.; Martel, L.; Lopez Honorato, E.; Farnan, I.; Vitova, T.; Somers, J.
Structure of $UC_2$ and $U_2C_3$:XRD, $^{13}C$ NMR and EXAFS study
2014. Journal of alloys and compounds, 589, 234–239.
doi:10.1016/j.jallcom.2013.11.202

**Lizenzinformationen: CC BY-NC-ND 4.0**